

# Multi-Response Optimization of Friction-Stir-Welded AA1100 Aluminum Alloy Joints

S. Rajakumar and V. Balasubramanian

(Submitted February 10, 2011; in revised form April 20, 2011)

**AA1100 aluminum alloy has gathered wide acceptance in the fabrication of light weight structures. Friction stir welding process (FSW) is an emerging solid state joining process in which the material that is being welded does not melt and recast. The process and tool parameters of FSW play a major role in deciding the joint characteristics. In this research, the relationships between the FSW parameters (rotational speed, welding speed, axial force, shoulder diameter, pin diameter, and tool hardness) and the responses (tensile strength, hardness, and corrosion rate) were established. The optimal welding conditions to maximize the tensile strength and minimize the corrosion rate were identified for AA1100 aluminum alloy and reported here.**

**Keywords** alloys, hardness, welding

## 1. Introduction

Friction stir welding (FSW) is a relatively new solid-state joining technique and has been extensively employed for aluminum alloys fabrication. Compared to conventional fusion welding methods, the advantages of the FSW process include better mechanical properties, low residual stress and distortion, and reduced occurrence of defects (Ref 1, 2). This welding technique is being applied to the aerospace, automotive, and shipbuilding industries, and it is attracting an increasing amount of research interest. FSW technology requires a thorough understanding of the process and the consequent evaluation of weld mechanical properties are needed to use the FSW process for production of components and structures. For this reason, detailed research and qualification work are required (Ref 3).

It is well known that whatever the welding method, the main challenge for the manufacturer is selecting the optimum welding parameters that would produce an excellent welded joint. To predict the optimum welding parameters accurately without consuming time, materials, and labor effort, various methods are available and one such method is response surface methodology (RSM).

Vijayan (Ref 4) reported the optimization of FSW process parameters for AA5083 aluminum alloy with multiple responses based on orthogonal array with gray relational analysis. The authors found the optimum levels of the process parameters to attain maximum tensile strength and minimum power consumption. Sarsilmaz (Ref 5) studied the effect of

FSW parameters such as spindle rotational speed, traverse speed, and stirrer geometry on ultimate tensile strength (UTS) and hardness of welded joints. In this article, the authors used the full-factorial experimental design to obtain the response measurements. Analysis of variance (ANOVA) and main effect plot was used to determine the significant parameters and set the optimal level for each parameter. A linear regression equation was also developed to predict each output characteristic.

Tansel et al. (Ref 6) adopted the genetically optimized neural network system (GONNS) to estimate the optimal operating condition of the FSW process. Five separate ANNs represented the relationship between two identical input parameters and each one of the considered characteristics of the welding zone. GA searched for the optimized parameters to make one of the parameters maximum or minimum, while the other four are kept within the desired range. Rajakumar et al. (Ref 7) proposed models using RSM to investigate the effect of FSW process parameters and weld parameters on the tensile strength of AA7075 aluminum alloy. In this article, the authors was developed an establish an empirical relationship between the FSW process and tool parameters and tensile strength of the joint using statistical tools such as design of experiments, analysis of variance, and regression analysis. The developed empirical relationship can be effectively used to predict the tensile strength of FSW joints at the 95% confidence level. Jayaraman et al. (Ref 8) have developed an empirical relationship for base metal properties and optimized FSW parameters on cast aluminum alloys. They developed relationships can be effectively used to predict the optimum FSW process parameters to fabricate defect-free joints with high tensile strength from the known base metal properties of cast aluminum alloys.

There have been lot of efforts to understand the effect of process parameters on material flow behavior, microstructure formation, and mechanical properties of friction stir welded joints. Finding the most effective parameters on properties of friction stir welds as well as realizing their influence on the weld properties has been major topics for researchers (Ref 9-12). The optimization of some of the important parameters, such as

S. Rajakumar and V. Balasubramanian, Department of Manufacturing Engineering, Center for Materials Joining & Research (CEMAJOR), Annamalai University, Annamalainagar, Chidambaram, 608002 Tamil Nadu, India. Contact e-mails: srkcemajor@yahoo.com, visvabalu@yahoo.com and balasubramanian.v.2784@annamalaiuniversity.ac.in.

axial tool pressure ( $F$ ), rotational speed ( $N$ ), and traverse speed ( $S$ ), on weld properties have been investigated. The combined effects of process parameters and tool parameters on multi-responses like tensile strength, hardness, and corrosion rate are hitherto not reported. It is important to investigate the mechanical properties of welded joint to describe its performance and the tensile strength and hardness are the most vital mechanical properties. In this investigation, along with the tensile strength and hardness, the corrosion rate also considered to evaluate the performance of the FSW joints of AA1100 alloy. Therefore, the first aim is to employ RSM to develop empirical relationships relating the FSW input parameters (rotational speed, welding speed, axial force, shoulder diameter, pin diameter, and tool hardness) and the three output responses (i.e., tensile strength, hardness, and corrosion rate). The second aim is to find the optimal welding combination that would maximize both the tensile strength and the hardness and minimize the corrosion rate.

## 2. Methodology

### 2.1 Response Surface Methodology

Engineers often wish to determine the values of the input process parameters at which the responses reach their optimum. The optimum could be either a minimum or a maximum of a particular function in terms of the process input parameters. Response surface methodology (RSM) is a collection of mathematical and statistical technique useful for analyzing problems in which several independent variables influence a dependent variable or response and the goal is to optimize the response (Ref 13). In many experimental conditions, it is possible to represent the independent factor in quantitative form as given in Eq 1. Then these factors can be thought of having a functional relationship or response as follows:

$$Y = \Phi(x_1, x_2, \dots, x_k) \pm e_r \quad (\text{Eq 1})$$

Between the response  $Y$  and  $x_1, x_2, \dots, x_k$  of  $k$  quantitative factors, the function  $\Phi$  is called response surface or response function. The residual  $e_r$  measures the experimental errors. For a given set of independent variables, a characteristic surface is responded. When the mathematical form of  $\Phi$  is not known, it can be approximate satisfactorily within the experimental region by polynomial. In the present investigation, RSM is applied to developing the mathematical model in the form of multiple regression equations for the quality characteristic of the friction stir welded AA1100 aluminum alloy. In applying the response surface methodology, the independent variable was viewed as a surface to which a mathematical model is fitted.

Representing the tensile strength of the joint by “ $Y$ ,” the response is a function of tool rotational speed ( $N$ ), welding speed ( $S$ ), axial force ( $F$ ), tool shoulder diameter ( $D$ ), tool pin diameter ( $P$ ), and tool hardness ( $H$ ) and it can be expressed as:

$$Y = f(\text{rotational speed, welding speed, axial force, shoulder diameter, pin diameter, tool hardness})$$

$$Y = f(N, S, F, D, P, H)$$

The second-order polynomial (regression) equation used to represent the response surface “ $Y$ ” is given by (Ref 14):

$$Y = b_0 + \sum b_i x_i + \sum b_{ii} x_i^2 + \sum b_{ij} x_i x_j + e_r \quad (\text{Eq 2})$$

### 2.2 Experimental Design

The test was designed based on a six factors, five levels central composite rotatable design with half replication (Ref 13). The friction stir-welding input variables are rotational speed, welding speed, axial force, shoulder diameter, pin diameter, and tool hardness. In order to find the range of each process and tool input parameters, trial weld runs were performed by changing one of the process parameters at a time. Absence of macro-level welding defects, smooth and uniform welded surface with the sound face were the criteria of selecting the feasible working range. Table 1 displays the macrographs to provide the evidence for fixing the feasible working range of welding parameters. Table 2 shows the process variables, their coded and actual values. Statistical software Design-Expert V8 was used to code the variables and to establish the design matrix (shown in Table 3). RSM was applied to the experimental data using the same software, polynomial Eq 2 was fitted to the experimental data to obtain the regression equations for all responses. The statistical significance of the terms in each regression equation was examined using the sequential  $F$  test, lack-of-fit test, and other adequacy measures using the same software to obtain the best fit.

### 2.3 Desirability Approach










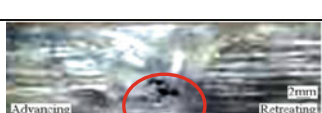

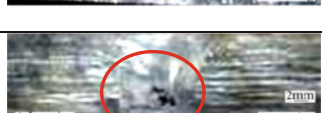
There are many statistical techniques for solving multiple response problems like overlaying the contours plot for each response, constrained optimization problems, and desirability approach. The desirability method is preferred due to its simplicity, availability in the software and provides flexibility in weighting and giving importance for individual response. Solving such multiple response optimization problems using this technique involves for combining multiple responses into a dimensionless measure of performance called the overall desirability function. The desirability approach involves transforming each estimated response,  $Y_i$ , into a unitless utility bounded by  $0 < d_i < 1$ , where a higher  $d_i$  value indicates that response value  $Y_i$  is more desirable, if  $d_i = 0$  this means a completely undesired response (Ref 15).

In this study, the individual desirability of each response,  $d_i$ , was calculated using Eq 3-6. The shape of the desirability function can be changed for each goal by the weight field “ $wt_i$ .” Weights are used to give more emphasis to the upper/lower bounds or to emphasize the target value. Weights could be ranged between 0.1 and 10; a weight greater than 1 gives more emphasis to the goal, while weights less than 1 give less emphasis. When the weight value is equal to 1, this will make the  $d_i$  vary from 0 to 1 in a linear mode. In the desirability objective function ( $D$ ), each response can be assigned an importance ( $r$ ), relative to the other responses. Importance varies from the least important value of 1, indicated by (+), the most important value of 5, indicated by (++++). If the varying degrees of importance are assigned to the different responses, the overall objective function is shown in Eq 7 below. Where  $n$  is the number of responses in the measure and  $T_i$  is the target value of  $i$ th response (Ref 16).

For goal of maximum, the desirability will be defined by:

$$d_i = \begin{cases} 0, & Y_i \leq \text{Low}_i \\ \left( \frac{Y_i - \text{Low}_i}{\text{High}_i - \text{Low}_i} \right)^{wt_i}, & \text{Low}_i < Y_i < \text{High}_i \\ 1, & Y_i \geq \text{High}_i \end{cases} \quad (\text{Eq 3})$$

**Table 1 Macrostructure observation of AA1100 aluminum alloy**

Input parameters	Parameter range	Macrostructure	Name of the defect	Probable reason
Rotational speed	<550 rpm		Tunnel defect	In sufficient heat generation and insufficient metal transportation
	>1100 rpm		Pin hole	Further increase in turbulence of the plasticized metal
Welding speed	<40 mm/min		Tunnel defect	Excess heat input per unit length of the weld and no vertical movement of the metal
	>160 mm/min		Tunnel defect	Increase in welding speed resulted in poor plasticization of metal
Axial force	<4 kN		Pin hole	In sufficient axial force and in adequate heat generation
	>9 kN		Worm hole	Additional axial force leads to excess heat input and thinning of the weld zone
Shoulder diameter	<7 mm		Kissing bond	Insufficient stirring butt surfaces could be directly bonded without the metallic bond between oxide free surfaces in the root part of the weld
	>21.5 mm		Pin hole	Excessive heat input due to softening and work hardening effect
Pin diameter	<2.5 mm		Piping defect	Asymptote heat generation and insufficient metal transportation
	>7.5 mm		Groove defect	Excessive heat input due to softening
Tool hardness	<33 HRc		Pin hole	Due to low frictional heat generation
	>56 HRc		Worm hole	High frictional heat generation

**Table 2 Important FSW parameters and their levels for AA1100 aluminum alloy**

#	Parameter	Notation	Unit	Levels				
				(−2.378)	(−1)	(0)	(+1)	(+2.378)
1	Rotational speed	<i>N</i>	rpm	562	700	800	900	1037
2	Welding speed	<i>S</i>	mm/min	40.54	75	100	125	159.5
3	Axial force	<i>F</i>	kN	3.62	5	6	7	8.37
4	Shoulder diameter	<i>D</i>	mm	7.86	12	15	18	22.13
5	Pin diameter	<i>P</i>	mm	2.6	4	5	6	7.37
6	Tool hardness	<i>H</i>	HRC	33	40	45	50	56

For goal of minimum, the desirability will be defined by:

$$d_i = \begin{cases} 1, & Y_i \leq \text{Low}_i \\ \left( \frac{\text{High}_i - Y_i}{\text{High}_i - \text{Low}_i} \right)^{wf_i}, & \text{Low}_i < Y_i < \text{High}_i \\ 0, & Y_i \geq \text{High}_i \end{cases} \quad (\text{Eq 4})$$

For goal as a target, the desirability will be defined by:

$$d_i = \begin{cases} \left( \frac{Y_i - \text{Low}_i}{T_i - \text{Low}_i} \right)^{wf_{1i}}, & \text{Low}_i < Y_i < T_i \\ \left( \frac{Y_i - \text{High}_i}{T_i - \text{High}_i} \right)^{wf_{2i}}, & T_i < Y_i < \text{High}_i \\ 0, & \text{Otherwise} \end{cases} \quad (\text{Eq 5})$$

For goal within range, the desirability will be defined by:

$$d_i = \begin{cases} 1, & \text{Low}_i < Y_i < \text{High}_i \\ 0, & \text{Otherwise} \end{cases} \quad (\text{Eq 6})$$

$$D = \left( \prod_{i=1}^n d_i^{r_i} \right)^{1/\sum r_i} \quad (\text{Eq 7})$$

### 2.4 Optimization

The optimization part in Design-Expert software V8 searches for a combination of factor levels that simultaneously satisfy the requirements placed (i.e., optimization criteria) on each one of the responses and process factors (i.e., multiple-response optimization). Numerical and graphical optimization methods were used in this study by selecting the desired goals for each factor and response. As mentioned before, the numerical optimization process involves combining the goals into an overall desirability function (*D*). The numerical optimization feature in the design-expert package finds one point or more in the factors domain that would maximize this objective function. In a graphical optimization with multiple responses, the software defines regions where requirement simultaneously meet the proposed criteria. Also, superimposing or overlaying critical response contours can be defined on a contour plot. Then, a visual search for the best compromise becomes possible. In case of dealing with the many responses, it is recommended to run numerical optimization first; otherwise it is impossible to find out a feasible region. The graphical optimization displays the area of feasible response values in the factor space. Regions that do not fit the optimization criteria are shaded (Ref 16). Figure 1 shows flow chart of the optimization steps in the Design-Expert software.

### 3. Experimental Work

The rolled plates of 5 mm thickness, low strength AA1100 aluminum alloy was used as base metal. Chemical composition

and mechanical properties of the base metal are shown in Table 4. The metal was cut to the required size (300 × 150 mm) by power hacksaw cutting and milling. The square butt joint configuration (300 × 300 mm) was prepared to fabricate FSW joints. The initial joint configuration was obtained by securing the plates in position using mechanical clamps. The direction of welding was normal to the rolling direction. Single-pass welding procedure was followed to fabricate the joints. Non-consumable tools made of high carbon steel were used to fabricate the joints. Based on six factors, five level central composite designs, 15 tools were made with different tool pin diameters, shoulder diameters, and tool hardnesses. Five levels of tool hardness were obtained by heat treating high carbon steel in different quenching media (air, oil, water, furnace cooling). An indigenously designed and developed computer numerical controlled friction stir welding machine (22 kW; 4000 RPM; 6 Ton) was used to fabricate the joints. As prescribed by the design matrix, 52 joints were fabricated. The tensile specimens comprising the welded joints were machined to the required dimensions (Fig. 2) as per ASTM E8M-04 guidelines (Ref 17). The tensile test was carried out in 100 kN, servo controlled universal testing machine (Make: FIE-BLUESTAR, India, Model: UNITEK 94100) with a cross head speed of 0.5 mm/min at room temperature. At each experimental condition, three specimens were tested and average of three results is presented in Table 2. The images of the specimens before and after the tensile test are shown in Fig. 3. Vickers's microhardness testing machine (Make: Shimadzu and Model: HMV-2T) was employed for measuring the hardness of the weld nugget region with 0.05 kg load at 15 s of dwell time. The corrosion test specimen of 10 × 10 × 5 mm (length × width × thickness) dimensions was extracted from the friction stir welded nugget region. Figure 4 shows specimens used in corrosion test. The specimen surfaces were ground using 500<sup>#</sup>, 800<sup>#</sup>, 1200<sup>#</sup>, 1500<sup>#</sup> grit SiC paper and cleaned with acetone and distilled water and then dried by flowing air. The initial weight (*w*<sub>0</sub>) of the specimen was measured before immersion to the solution of 3.5% NaCl solution. After 24 h of immersion, specimens were taken out and corrosion products were removed by immersing the specimens for 5–10 min in a specially prepared solution (50 mL phosphoric acid (H<sub>3</sub>PO<sub>4</sub>, spgr1.69) 20 g chromium trioxide (CrO<sub>3</sub>) Reagent water to make 1000 mL. The final weight (*W*<sub>t</sub>) of the specimen was measured and the net weight loss was calculated. The corrosion rate was calculated using the following equation (Ref 18).

$$\text{Corrosion rate (CR)} = \frac{87.6 \times W}{A \times D \times T} \quad (\text{Eq 8})$$

where *W* is the weight loss in mg, *A* is the surface area of the specimen in cm<sup>2</sup>, *D* is the density of the material, 2.7 g/cm<sup>3</sup>, *T* is the exposure time in hours.



**Table 3** Experimental design matrix and results

Exp. no	Experimental details						Results		
	Input parameters						Responses		
	Rotational speed	Welding speed	Axial force	Shoulder diameter	Pin diameter	Tool hardness	TS, MPa	H, HV	CR, (mm/y) × 10 <sup>-4</sup>
1	-1	-1	-1	-1	-1	-1	69	35	6.09
2	1	-1	-1	-1	-1	1	89	52	3.9
3	-1	1	-1	-1	-1	1	75	40	4.53
4	1	1	-1	-1	-1	-1	90	53	3.68
5	-1	-1	1	-1	-1	1	85	49	5.73
6	1	-1	1	-1	-1	-1	96	58	4.93
7	-1	1	1	-1	-1	-1	82	46	5.04
8	1	1	1	-1	-1	1	99	61	3.5
10	-1	-1	-1	1	-1	1	80	44	5.29
11	1	-1	-1	1	-1	-1	85	49	3.07
12	-1	1	-1	1	-1	-1	76	41	4.22
13	1	1	-1	1	-1	1	89	52	3
14	-1	-1	1	1	-1	-1	77	42	5.18
15	1	-1	1	1	-1	1	92	55	4
16	-1	1	1	1	-1	1	86	50	4.94
17	1	1	1	1	-1	-1	97	59	3.76
18	-1	-1	-1	-1	1	1	77	42	5.56
19	1	-1	-1	-1	1	-1	85	49	4.62
20	-1	1	-1	-1	1	-1	73	38	6.1
21	1	1	-1	-1	1	1	88	51	3.74
22	-1	-1	1	-1	1	-1	76	41	6.03
23	1	-1	1	-1	1	1	93	56	3.79
24	-1	1	1	-1	1	1	84	48	4.99
25	1	1	1	-1	1	-1	98	60	4
26	-1	-1	-1	1	1	-1	81	45	3.83
27	1	-1	-1	1	1	1	94	57	1.82
28	-1	1	-1	1	1	1	90	53	4.1
29	1	1	-1	1	1	-1	99	61	2.82
30	-1	-1	1	1	1	1	89	52	3.97
31	1	-1	1	1	1	-1	95	58	2.62
32	-1	1	1	1	1	-1	90	53	4.39
33	-2.38	0	0	0	0	0	80	44	6.09
34	2.38	0	0	0	0	0	105	66	5.11
35	0	-2.38	0	0	0	0	83	47	2.99
36	0	2.38	0	0	0	0	90	53	4.61
37	0	0	-2.38	0	0	0	83	47	4
38	0	0	2.38	0	0	0	97	59	3.75
39	0	0	0	-2.38	0	0	82	46	4.49
40	0	0	0	2.38	0	0	90	53	5.07
41	0	0	0	0	-2.38	0	85	49	2.53
42	0	0	0	0	2.38	0	91	54	3.53
43	0	0	0	0	0	-2.38	81	45	2.82
44	0	0	0	0	0	2.38	87	51	4.38
45	0	0	0	0	0	0	101	63	3.49
46	0	0	0	0	0	0	100	62	0.73
47	0	0	0	0	0	0	101	63	0.74
48	0	0	0	0	0	0	102	63	0.76
49	0	0	0	0	0	0	101	64	0.43
50	0	0	0	0	0	0	99	61	0.47
51	0	0	0	0	0	0	98	60	0.37
52	0	0	0	0	0	0	103	64	0.71

TS, tensile strength; H, hardness; CR, corrosion rate

#### 4. Development of Empirical Relationships

The fit summary tab in the Design-Expert software suggests the highest order of polynomial where the additional terms are significant and the model is not aliased. The tensile strength,

hardness, and corrosion rate of the weld nugget of FSW joints are function of rotational speed ( $N$ ), welding speed ( $S$ ), axial force ( $F$ ), shoulder diameter ( $D$ ), pin diameter ( $P$ ), and tool hardness ( $H$ ) and it can be expressed as:

$$\text{Tensile strength (TS)} = f(N, S, F, D, P, H) \quad (\text{Eq 9})$$

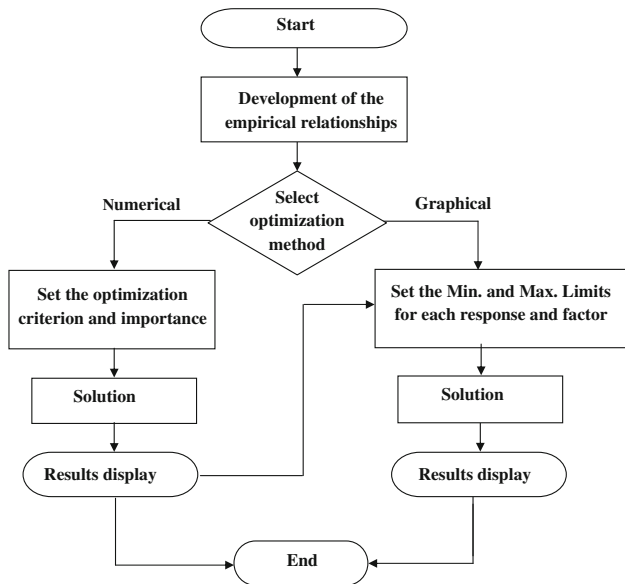


Fig. 1 Flow chart for optimization steps

$$\text{Weld Nugget hardness (WH)} = f(N, S, F, D, P, H) \quad (\text{Eq 10})$$

$$\text{Corrosion rate (CR)} = f(N, S, F, D, P, H) \quad (\text{Eq 11})$$

and for six factors, the selected polynomial could be expressed as:

$$\begin{aligned}
 (\text{TS})\text{or}(\text{WH})\text{or}(\text{CR}) &= b_0 + b_1(N) + b_2(S) + b_3(F) + b_4(D) + b_5(P) + b_6(H) \\
 &+ b_{11}(N^2) + b_{22}(S^2) + b_{33}(F^2) + b_{44}(D^2) + b_{55}(P^2) \\
 &+ b_{66}(H^2) + b_{12}(NS) + b_{13}(NF) + b_{14}(ND) + b_{15}(NP) \\
 &+ b_{16}(NH) + b_{23}(SF) + b_{24}(SD) + b_{25}(SP) + b_{26}(SH) \\
 &+ b_{34}(FD) + b_{35}(FP) + b_{36}(FH) + b_{45}(DP) + b_{46}(DH) \\
 &+ b_{56}(PH) \quad (\text{Eq 12})
 \end{aligned}$$

where  $b_0$  is the average of responses and  $b_1, b_2, \dots, b_{66}$  are the coefficients that depend on respective main and interaction effects of the parameters. The value of the coefficient was calculated using the following expressions,

$$b_0 = 0.110749 \left( \sum y \right) - 0.018738 \sum (X_{iij}) \quad (\text{Eq 13})$$

Table 4 Chemical composition (wt.%) and mechanical properties of base metal

Chemical composition							Mechanical properties			
Alloy	Si	Fe	Cu	Mn	Mg	Al	Yield strength, MPa	Ultimate tensile strength, MPa	Elongation, %	Hardness (0.05 kg @ 15 s), HV
AA1100	0.004	0.061	0.0015	0.508	0.152	Bal	105	110	32	61

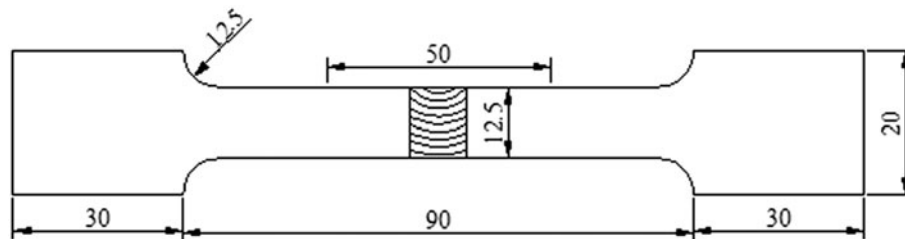
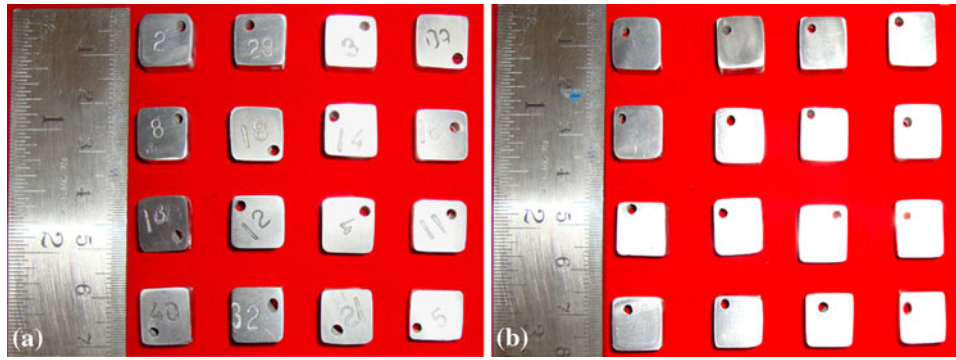


Fig. 2 Dimensions of flat tensile specimens (in mm)



Fig. 3 Tensile specimens. (a) Before and (b) after tensile test



**Fig. 4** Corrosion specimens. (a) Before and (b) after corrosion

$$b_i = 0.023087 \sum (X_{iy}) \quad (\text{Eq 14})$$

$$b_{ii} = 0.0152625 \sum (X_{iiv}) + 0.001217 \sum \sum (X_{iiv}) - 0.018738 \left( \sum y \right) \quad (\text{Eq 15})$$

$$b_{ij} = 0.03125 \sum (X_{ijv}) / n \quad (\text{Eq 16})$$

All the coefficients were tested for their significance at 95% confidence level applying Fisher's  $F$  test using Design-Expert V8 statistical software package. After determining the significant coefficients, the final models were developed using only these coefficients and the final empirical relationships to estimate tensile strength, hardness, and corrosion rate of weld nugget, developed by the above procedures are given below:

(i) *Tensile strength*

$$\begin{aligned} (\text{TS}) = \{ & 100.65 + 5.81(N) + 1.45(S) + 2.89(F) + 1.69(D) \\ & + 1.21(P) + 1.11(H) - 1.31(ND) - 0.69(NP) \\ & - 1.56(NH) - 1.13(SH) - 1.31(FD) - 0.94(FP) \\ & + 1.88(DP) - 1.49(N^2) - 2.56(S^2) - 1.94(F^2) \\ & - 2.64(D^2) - 2.29(P^2) - 3.00(H^2) \} \text{MPa.} \quad (\text{Eq 17}) \end{aligned}$$

(ii) *Weld Nugget hardness*

$$\begin{aligned} (\text{WH}) = \{ & 62.52 + 5.09(N) + 1.21(S) + 2.55(F) + 1.49(D) \\ & + 1.06(P) + 1.02(H) - 1.06(ND) - 0.50(NP) \\ & - 1.38(NH) - 0.94(SH) - 1.13(FD) - 0.81(FP) \\ & + 1.63(DP) - 1.37(N^2) - 2.25(S^2) - 1.72(F^2) \\ & - 2.34(D^2) - 1.98(P^2) - 2.60(H^2) \} \text{HV.} \quad (\text{Eq 18}) \end{aligned}$$

(iii) *Corrosion rate*

$$\begin{aligned} (\text{CR}) = \{ & 0.65 - 0.68(N) - 0.09(S) + 0.06(F) - 0.46(D) \\ & - 0.12(P) - 0.09(H) + 0.09(NS) + 0.08(NF) \\ & + 0.17(SD) + 0.20(SP) + 0.15(FD) - 0.07(FP) \\ & - 0.29(DP) + 0.13(DH) - 0.10(PH) + 0.88(N^2) \\ & + 0.56(S^2) + 0.53(F^2) + 0.65(D^2) + 0.43(P^2) \\ & + 0.53(H^2) \} \text{mm/y.} \quad (\text{Eq 19}) \end{aligned}$$

The adequacy of the developed empirical relationships was tested using the analysis of variance (ANOVA) technique

**Table 5** ANOVA test results

Terms	Tensile strength (TS)	Weld Nugget hardness (WH)	Corrosion rate (CR)
First-order terms			
Sum of squares (SS)	2152.94	2152.94	$3.08 \times 10^{-7}$
Degrees of freedom (df)	6	6	6
Mean squares (MS)	358.82	358.82	$5.14 \times 10^{-7}$
Second-order terms			
Sum of squares (SS)	3923.405	3923.405	$1.30 \times 10^{-6}$
Degrees of freedom (df)	27	27	27
Mean squares (MS)	145.3113	145.3113	$4.82 \times 10^{-8}$
Error order terms			
Sum of squares (SS)	17.875	17.875	$2.91 \times 10^{-9}$
Degrees of freedom (df)	7	7	7
Mean squares (MS)	2.553571	2.553571	$4.16 \times 10^{-10}$
Lack of fit			
Sum of squares (SS)	23.546	23.546	$5.19 \times 10^{-8}$
Degrees of freedom (df)	17	17	17
Mean squares (MS)	1.385102	1.385102	$3.05 \times 10^{-9}$
$F$ ratio	2.37	2.37	2.37
Prob > $F$	84.19424	84.19424	142.6737
$R^2$	0.989553	0.989553	99.3%
$R_{\text{ratio}}$ (calculated)	0.9529	0.9529	97.2%
$R_{\text{ratio}}$ (from table) (33,7,0.05)	2.30	2.30	2.30
Model	Significant	Significant	Significant

$F$ , Fisher's ratio

(Ref 13). Table 5 shows the ANOVA results for the tensile strength, hardness, and corrosion rate, respectively. As per this technique, if the calculated value of the  $F$ -ratio of the developed model is less than the standard  $F$  ratio (from  $F$  table) value at a desired level of confidence (say 95%), then the model is said to be adequate within the confidence limit.

## 5. Effect of Process and Tool Parameters on the Responses

In the following sections, whenever an interaction effect or a comparison between any two input parameters is being discussed the other parameters are at center (middle) level.

## 5.1 Tensile Strength

Perturbation plot shown in Fig. 5 illustrates the effect of the friction stir welding parameters on the tensile strength for an optimization design. This graph shows how the response changes as each factor moves from a chosen reference point, with all other factors held constant at the reference value (Ref 19). A steep slope or curvature in a factor indicates that the response is sensitive to that factor. From the plot it can be observed that the tool rotational speed is most influential factor on tensile strength of the joint followed by tool hardness, axial force, shoulder diameter, pin diameter, and then welding speed. Figure 6 is a contour graph shows the effect of the rotational speed and shoulder diameter on the tensile strength. When rotational speed is compared with the shoulder diameter (at a constant tool hardness of 45 HRc, axial force of 6 kN, pin diameter of 5 mm, and welding speed of 100 mm/min) rotational speed is more sensitive to changes in tensile strength as illustrated in Fig. 6.

The interaction effect between the rotational speed and the shoulder diameter is more significant than the interaction effect between the other combinations of parameters. In FSW, the tool rotational speed is more sensitive factor than other parameters. Especially, heat generation due to friction is mainly dependent on tool rotational speed. The friction between the shoulder and

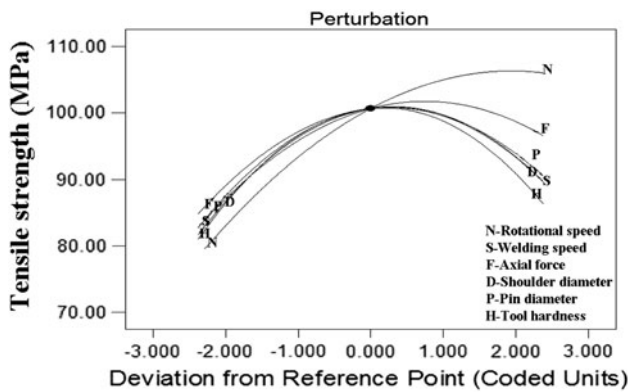


Fig. 5 Perturbation plot showing the effect of all factors on the tensile strength

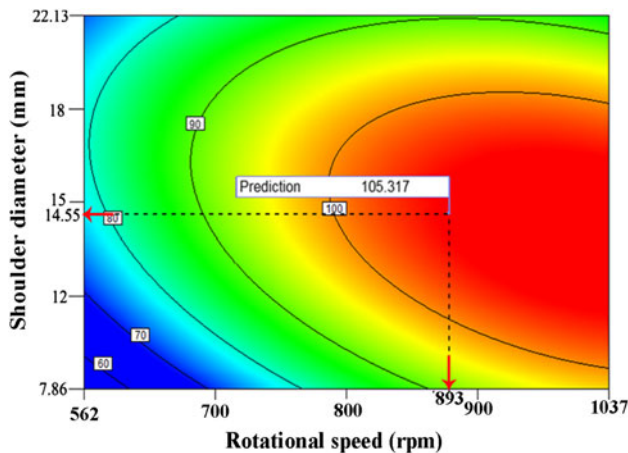


Fig. 6 Contours plot showing the effect of  $N$  and  $D$  on the tensile strength at  $S = 100$  mm/min,  $F = 6$  kN,  $P = 5$  mm,  $H = 45$  HRc

work piece results in the biggest component of heating. From the heating aspect, the relative size of pin and shoulder is important. The shoulder also provides confinement for the heated volume of material. The second function of the tool shoulder is to 'stir' and 'move' the material. The uniformity of the microstructure and properties as well as process load is governed by the tool design (Ref 20). Larger shoulder diameter, leads to wider contact area and resulted in wider TMAZ region and HAZ region, subsequently the tensile strength of the joints are deteriorated. As the shoulder diameter increased from 9 to 15 mm both the strength and the hardness improved, reaching maximum before falling again at larger shoulder diameter (21 mm). The smaller shoulder diameter resulted in sufficient heat generation due to smaller contact area. The small contact area causes defects in friction stir welding zone causes grain growth and severe clustering of precipitates in the stir zone, which resultantly produced lower hardness in the stir zone. The lower tool rotational speed produces less heat generation (Ref 21, 22), irrespective of shoulder diameter, subsequently heat supplied to the base material is less, which causes insufficient material flow and less plasticization in stir zone and hence, the tensile strength is lower. The higher rotational speed produces high heat generation, irrespective of shoulder diameter, subsequently heat supplied to the base material is high, which causes turbulent material flow and grain coarsening in stir zone and hence the tensile strength is lower. Neither low heat input nor high heat input is preferred in FSW, due to the reduction in tensile strength of the joints and it is evident from Fig. 7.

## 5.2 Microhardness

Microhardness was measured at mid-thickness region of the weld nugget. The base metal recorded hardness of 61 HV, which is lower than stir zone. The hardness of the stir zone is considerably higher than that of the base metal irrespective of the tool rotational speed used. There are two main reasons for improved hardness in the stir zone. (i) The grain size of stir zone is much finer than that of base metal. The grain refinement plays an important role in material strengthening. According to the Hall-Petch equation, hardness increases as the grain size decreases. (ii) The small intermetallic particles improve the hardness, according to the Orowan hardening mechanism (Ref 23). The difference in hardness between the heat affected zone and the stir zone is attributed to the grain refinement in the stir

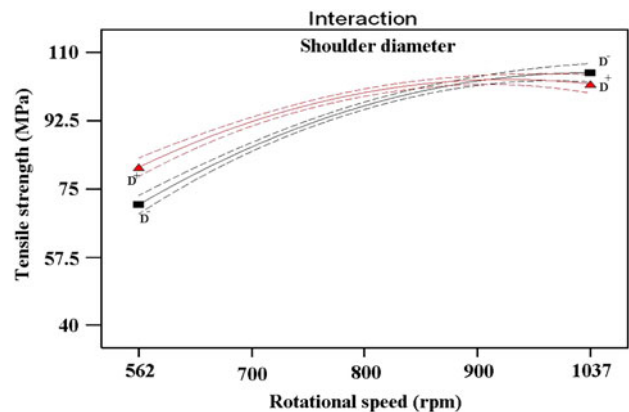
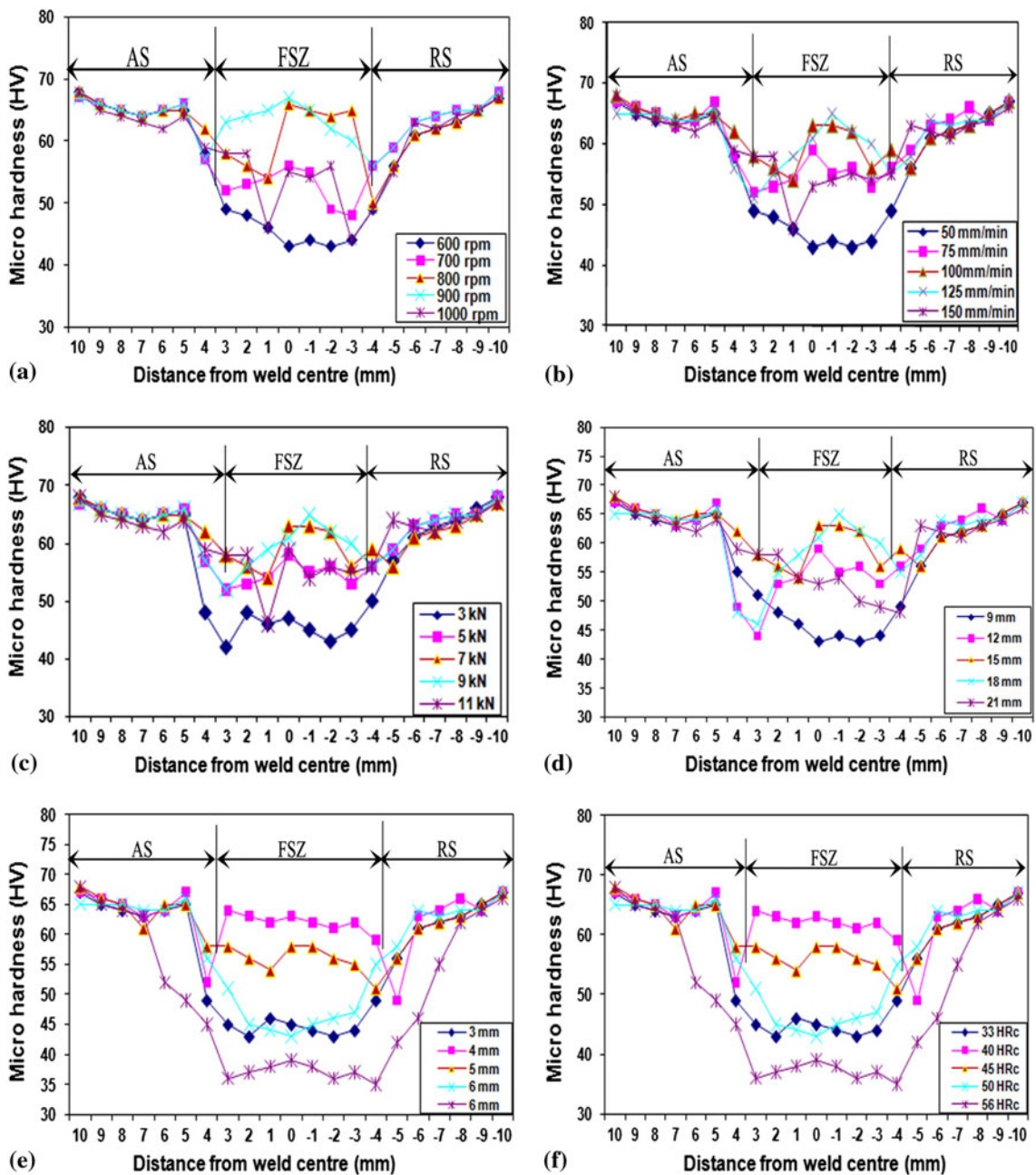


Fig. 7 Interaction effect between  $N$  and  $S$  on the tensile strength at  $F = 6$  kN,  $D = 15$  mm,  $P = 5$  mm,  $H = 45$  HRc





**Fig. 8** Effect of process and tool parameters on micro hardness of AA1100 aluminum alloy. (a) Tool rotational speed, (b) welding speed, (c) axial force, (d) shoulder diameter, (e) pin diameter, and (f) tool hardness

zone. Figure 8(a) shows the lowest hardness was recorded in the joint fabricated with a tool rotational speed of 600 rpm at the TMAZ region of retreating side. Retreating side (RS) recorded appreciably lower hardness values compared to advancing side (AS) irrespective of the tool rotational speed used. The joint fabricated with a tool rotational speed of 900 rpm recorded the highest hardness value of 67 HV in the stir zone region. Similarly, the welding speed of 125 mm/min (Fig. 8b), axial force of 9 kN (Fig. 8c), shoulder diameter of 18 mm (Fig. 8d), pin diameter of 4 mm (Fig. 8e), tool hardness of 40 HRC (Fig. 8f), resulted in maximum hardness compared to other process parameters, and this may be one of the reasons for superior strength properties of this joint.

### 5.3 Corrosion Rate

Although aluminum forms a protective aluminum oxide layer on the surface, this thin layer can be breached in aggressive environments leading to corrosion. In particular, NaCl containing environments lead to the formation of aluminum chlorides which in turn reduces the effectiveness of the oxide layer in preventing corrosion. For that reason, the effect of friction stir welding parameters on corrosion behavior of the welds was investigated. The results demonstrate that all the input parameters have a significant effect on the corrosion rate of the welded joint. Figure 9 shows a perturbation plot to compare the effect of different welding factors at a particular

point (mid-point by default) in the design space. From this figure, it can be noticed that the corrosion rate is minimum when the rotational speed is at middle level, whereas at lower welding speed and at higher rotational speed, the corrosion rate was maximum. This is because the high temperatures generated under these conditions have led to a grain growth in the weld nugget and TMAZ which have enhanced their corrosion rate.

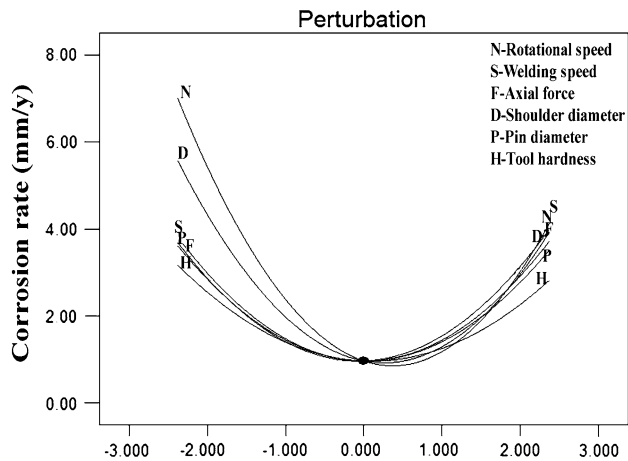


Fig. 9 Perturbation plot showing the effect of all factors on the corrosion rate

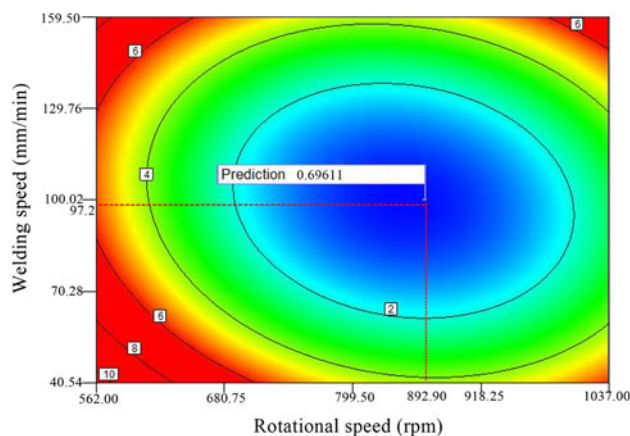


Fig. 10 Contours plot showing the effect of  $N$  and  $S$  on the corrosion rate at  $F = 6$  kN,  $D = 15$  mm,  $H = 45$  HRc

Similarly, the joint fabricated with the welding speed of 100 mm/min, an axial force of 6 kN, the joint fabricated using a tool with the shoulder diameter of 15 mm, pin diameter of 5 mm, and hardness of 45 HRc yielded the lower corrosion rate. The results demonstrated that the lowest corrosion rate could be obtained when all the FSW input parameters were in middle level, which is attributed to the breaking down and dissolution of the intermetallic particles (Ref 24). Figure 10 shows the effect of the rotational speed and shoulder diameter on the corrosion rate at a welding speed of 100 mm/min, axial force 6 kN, pin diameter 5 mm, and tool hardness 45 HRc. The results indicate that as the rotational speed increases, the corrosion rate decreases. This is important in the optimization of the welding process parameters.

## 6. Optimization

The issue of linking between the strength and the corrosion must be addressed as any increase in the strength is usually reflected in deteriorating the corrosion. As a consequence both strength and corrosion are usually studied together. On balance, and based on the above discussion, it is better to run an optimization study to find out the optimal welding conditions at which the desirable mechanical properties of the welded joint can be achieved. In fact, once the models have been developed and checked for adequacy, the optimization criteria can be set to find out the optimum welding conditions. In this investigation, two criteria were implemented to maximize both the tensile strength and the hardness. The first criteria were to reach the maximum tensile strength and hardness with no limitation on either the welding parameters or the corrosion rate. While, in the second criteria the goal was to reach the maximum tensile strength and hardness at relatively low-corrosion rate using maximum rotational speed and welding speed. However, Table 6 summarizes these two criteria. While Table 7 and 8 presents the optimal solution based on the two optimization criteria is determined by design-expert software. The optimization results clearly demonstrated that whatever the optimization criteria, the rotational speed has to be around its center limit of 900 rpm to achieve the maximum tensile and hardness. This result supports the discussion made earlier on the effect of rotational speed on the responses. Table 7 presents the optimal welding conditions according to the first criteria that would lead to the maximum tensile and hardness of about 105 MPa and 67 HV respectively, at high corrosion rate of about

Table 6 Optimization criteria used in this study

Parameter or responses	Limits		Importance	First criterion	Second criterion
	Lower	Upper			
Rotational speed, rpm	700	900	3	In range	Maximize
Welding speed, mm/min	75	125	3	In range	In range
Axial force, kN	5	7	3	In range	In range
Shoulder diameter, mm	12	18	3	In range	In range
Pin diameter, mm	4	6	3	In range	In range
Tool hardness, HRc	45	50	3	In range	Maximize
Tensile strength, MPa	69	105	5	Maximize	Maximize
Hardness, HV	35	66	5	Maximize	Maximize
Corrosion rate, mm/y	$0.37 \times 10^{-4}$	$6.09 \times 10^{-4}$	3	In range	Minimize

**Table 7 Optimal solution as obtained by design-expert based on the first criterion**

Exp. no	Experimental details						Results			
	Input parameters						Responses			
	Rotational speed, rpm	Welding speed, mm/min	Axial force, kN	Shoulder diameter, mm	Pin diameter, mm	Tool hardness, HRc	TS, MPa	H, HV	CR, (mm/y) × 10 <sup>-4</sup>	Desirability
1	892.90	97.21	6.84	14.56	5.12	43.37	105.317	66.5212	0.69635	1
2	876.64	108.01	6.50	14.85	4.88	45.38	105.253	66.4778	0.627	1
3	871.15	102.31	6.67	14.78	4.97	43.54	105.004	66.2545	0.627	1
4	894.99	102.87	6.11	16.04	5.28	43.08	105.004	66.3142	0.68217	1
5	886.37	118.13	6.70	16.02	5.10	43.77	105.251	66.4472	0.72116	1
6	876.70	107.41	6.29	14.66	5.15	44.79	105.026	66.2845	0.65482	1
7	887.67	117.15	6.34	15.18	5.06	42.33	105.003	66.1786	0.65639	1
8	893.94	99.72	6.56	15.80	5.43	45.93	105.008	66.3716	0.6842	1
9	871.75	105.75	6.81	14.94	5.08	44.22	105.302	66.5233	0.69432	1
10	890.22	105.57	6.22	16.24	5.09	43.36	105.086	66.3667	0.6998	1
11	897.27	101.15	6.26	14.56	4.94	42.77	105.096	66.307	0.6873	1
12	898.87	105.49	6.05	15.74	5.47	45.43	105.046	66.3657	0.69027	1
13	897.11	95.38	6.93	14.75	5.08	44.49	105.413	66.6275	0.74653	1
14	887.58	103.60	6.34	14.55	4.74	43.31	105.042	66.2461	0.64776	1
15	881.19	107.40	6.39	14.99	4.66	43.85	105.015	66.2338	0.69261	1

**Table 8 Optimal solution as obtained by design-expert based on the second criterion**

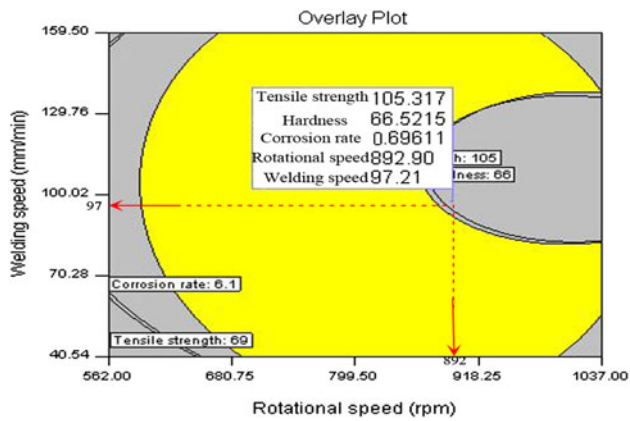
Exp. no	Experimental details						Results			
	Input parameters						Responses			
	Rotational speed, rpm	Welding speed, mm/min	Axial force, kN	Shoulder diameter, mm	Pin diameter, mm	Tool hardness, HRc	TS, MPa	H, HV	CR, (mm/y) × 10 <sup>-4</sup>	Desirability
1	900.00	100.52	6.21	15.27	5.14	49.49	102.506	64.1775	1.52591	0.921229
2	900.00	100.57	6.21	15.31	5.14	49.47	102.536	64.2035	1.52341	0.921224
3	900.00	100.42	6.21	15.30	5.16	49.46	102.535	64.205	1.51899	0.921223
4	900.00	100.97	6.22	15.26	5.15	49.47	102.551	64.2162	1.53083	0.921215
5	900.00	100.34	6.20	15.25	5.15	49.50	102.48	64.155	1.52715	0.921215
6	900.00	100.15	6.22	15.33	5.15	49.54	102.448	64.1322	1.53558	0.921183
7	900.00	100.59	6.23	15.25	5.12	49.57	102.445	64.1238	1.55048	0.921181
8	900.00	100.33	6.21	15.28	5.17	49.38	102.62	64.2802	1.50802	0.921167
9	900.00	100.83	6.23	15.21	5.16	49.51	102.517	64.1879	1.53926	0.921166
10	900.00	100.16	6.21	15.25	5.13	49.60	102.38	64.0688	1.54799	0.921161
11	900.00	100.40	6.20	15.39	5.16	49.65	102.269	63.9778	1.54316	0.92106
12	900.00	100.01	6.24	15.14	5.10	49.52	102.535	64.1983	1.55278	0.921054
13	900.00	100.44	6.20	15.29	5.16	49.47	102.502	64.176	1.51319	0.921006
14	900.00	100.29	6.29	15.22	5.10	49.48	102.638	64.2913	1.56728	0.920903
15	900.00	100.64	6.20	15.26	5.15	49.15	102.889	64.5069	1.47087	0.920836

0.6963 × 10<sup>-4</sup> mm/y. But, if the corrosion rate is to be reduced much further with approximate percentage of 54 with acceptable tensile and the hardness, the rotational speed has to be maximized to its highest value and a welding speed of 100.52 mm/min has to be used instead of 97.21 mm/min. In this case, the tensile strength and hardness would be about 102 MPa and 62 HV at corrosion rate of about 1.52 × 10<sup>-4</sup> mm/y, respectively, as can be seen in Table 8. It is obvious that the graphical optimization allows visual selection of the optimum welding conditions according to certain criteria. The result of the graphical optimization is the overlay plots, this type of plots are extremely practical for quick technical use in the workshop to choose the values of the welding parameters

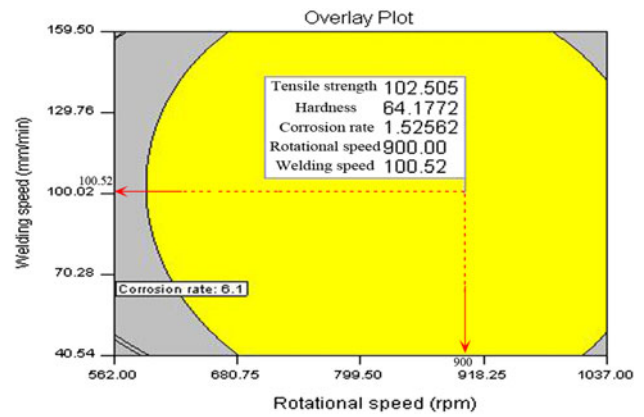
that would achieve certain response value for this type of material. The yellow/shaded areas on the overlay plots in Fig. 11 and 12 are the regions that meet the proposed criteria.

### 6.1 Validation of the Developed Models

To validate the developed models, three confirmation experiments were carried out with the welding conditions chosen randomly from the optimization results. For the actual responses the average of three measured results was calculated. Table 9 summarizes the experimental condition, the average of actual experimental values, the predicted values, and the



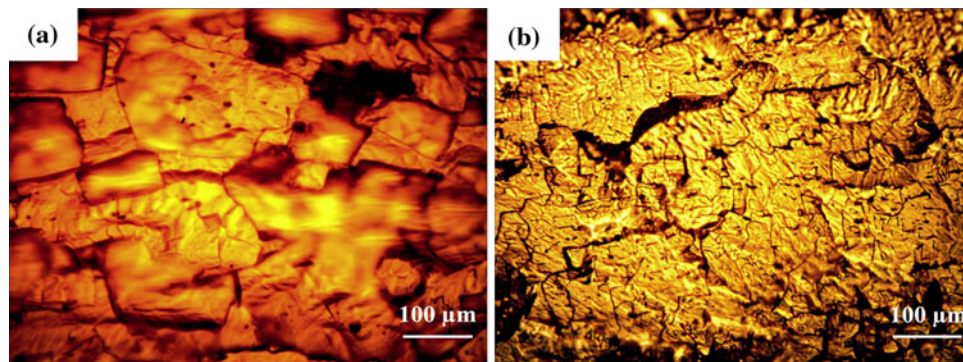
**Fig. 11** Overlay plot shows the region of optimal welding condition based on the first criterion at  $F = 6$  kN,  $D = 15$  mm,  $P = 5$  mm,  $H = 45$  HRc



**Fig. 12** Overlay plot shows the region of optimal welding condition based on the second criterion at  $F = 6$  kN,  $D = 15$  mm,  $P = 5$  mm,  $H = 45$  HRc

**Table 9** Validation test results

Exp. no	Experimental details						Results			
	Input parameters						Responses			
	Rotational speed, rpm	Welding speed, mm/min	Axial force, kN	Shoulder diameter, mm	Pin diameter, mm	Tool hardness, HRc	TS, MPa	H, HV	CR, (mm/y) $\times 10^{-4}$	
1	892.90	97.21	6.84	14.56	5.12	43.37	Actual	99	65	0.654
							Predicted	102.506	66.521	0.69635
							Error %	3.42	2.28	6.07
2	871.15	102.31	6.67	15.71	5.21	44.83	Actual	102	63	0.611
							Predicted	105.004	64.205	0.627
							Error %	2.86	1.87	2.55
3	886.37	118.13	6.70	16.02	5.10	43.77	Actual	101	61	0.689
							Predicted	105.251	64.155	0.72116
							Error %	4.04	4.91	4.45

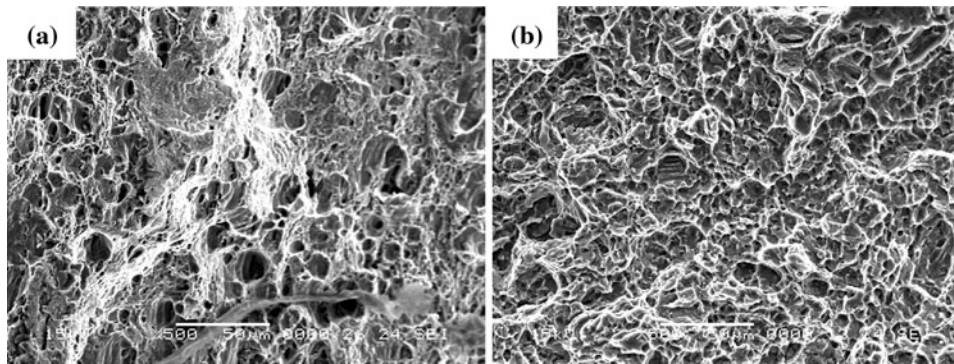


**Fig. 13** Optical micrographs. (a) Base metal and (b) stir zone (optimum condition)

percentages of error. The optimum values of process parameters and average tensile strength of friction stir welded AA1100 aluminum alloy was found to be 105 MPa, which shows the excellent agreement with the predicted values. The base metal micrograph of Fig. 13(a) contains a coarse and elongated grain. But in the traverse section of FSW joint fabricated using optimum parameters reveals that there is no defect due to

sufficient heat generation and contains finer grains in weld zone are shown in Fig. 13(b). The average grain diameter was measured in stir zone and it was found to be smaller (12  $\mu$ m), compare to base metal (85  $\mu$ m). The fracture surfaces of the tensile tested specimens were characterized using SEM to understand the failure patterns. All the fracture surfaces invariably consist of dimples, which is an indication that the





**Fig. 14** SEM fractographs of tensile specimens. (a) Base metal and (b) stir zone (optimum condition)

failure is the result of ductile fracture. The fracture surface of the base metal in Fig. 14(a) shows larger dimples than the stir zone Fig. 14(b).

## 7. Conclusions

1. The friction stir welding process and tool parameters were optimized using multi-objective optimization in the RSM to obtain the maximum strength and minimum corrosion rate.
2. A maximum tensile strength of 105 MPa, hardness value of 67 HV, and minimum corrosion rate of  $0.69 \times 10^{-4}$  in the stir zone region is exhibited by the FSW joints fabricated with the optimized parameters of 893 rpm rotational speed, 100 mm/min welding speed, 6.5 kN axial force, shoulder diameter of 14.8 mm, pin diameter of 4.9 mm, and tool material hardness of 45.4 HRC.
3. The corrosion rate of the welds can be reduced to a minimum with acceptable mechanical properties if the optimal welding conditions are used to fabricate the joints.
4. Rotational speed is more sensitive than other parameters followed by axial force, welding speed, shoulder diameter, pin diameter, and tool material hardness.

## Acknowledgments

The authors are grateful to the Department of Manufacturing Engineering, Annamalai University, Annamalai Nagar, India for extending the facilities of Material Testing Laboratory to carry out this investigation. The authors wish to place their sincere thanks to Clean Technology Division of Ministry of Environment and Forest, Government of India, New Delhi for financial support rendered through a R&D Project No. MoEF1-9/2005-CT.

## References

1. Thomas WM, Friction Stir Welding. International Patent Application No. PCT/ GB92/02203 and GB Patent Application No. 9125978.8. U.S. Patent No. 5 (1991) 460; 317
2. C.J. Dawes, An Introduction to Friction Stir Welding and its Development, *Weld. Met. Fabr.*, 1995, **63**, p 2–16
3. W.M. Thomas and E.D. Nicholas, Friction Stir Welding for the Transportation Industries, *Mater. Des.*, 1997, **18**, p 269–273
4. S. Vijayan, Multi objective Optimization of Friction Stir Welding Process Parameters on Aluminum Alloy AA 5083 Using Taguchi-Based Grey Relation Analysis, *Mater. Manuf. Proc.*, 2010, **25**, p 1206–1212
5. F. Sarsilmaz, Statistical Analysis on Mechanical Properties of Friction-Stir-Welded AA 1050/AA 5083 Couples, *Int. J. Adv. Manuf. Technol.*, 2009, **43**(3–4), p 248–255
6. I.N. Tansel, M. Demetgul, H. Okuyucu, and A. Yapici, Optimizations of Friction Stir Welding of Aluminum Alloy by Using Genetically Optimized Neural Network, *Int. J. Mach. Tool. Manuf.*, 2009, **44**, p 1205–1214
7. S. Rajakumar, C. Muralidharan, and V. Balasubramanian, Optimization of the Friction-Stir-Welding Process and the Tool Parameters to Attain a Maximum Tensile Strength of AA7075-T6 Aluminium Alloy, *J. Eng. Manuf.*, 2010, **224**, p 1175–1191
8. M. Jayaraman, R. Sivasubramanian, and V. Balasubramanian, Establishing Relationship Between the Base Metal Properties and Friction Stir Welding Process Parameters of Cast Aluminium Alloys, *Mater. Des.*, 2011, **31**, p 4567–4576
9. S. Lim, S. Kim, C.-G. Lee, and S. Kim, Tensile Behavior of Friction-Stir-Welded Al 6061-T651, *Metall. Mater. Trans. A*, 2004, **35**, p 2829–2835
10. K. Elangovan and V. Balasubramanian, Influences of Tool Pin Profile and Tool Shoulder Diameter on the Formation of Friction Stir Processing Zone in AA6061 Aluminium Alloy, *Mater. Des.*, 2008, **293**, p 362–373
11. A. Barcellona, G. Buffa, L. Fratini, and D. Palmeri, On Microstructural Phenomena Occurring in Friction Stir Welding of Aluminium Alloys, *J. Mater. Process. Technol.*, 2006, **177**, p 340–343
12. Y.S. Sato, H. Takauchi, S.H.C. Park, and H. Kokawa, Characteristics of the Kissing-Bond in Friction Stir Welded Al Alloy 1050, *Mater. Sci. Eng. A*, 2005, **405**, p 333–338
13. D.C. Montgomery, *Design and Analysis of Experiments*, 2nd ed., Wiley, New York, 1984
14. S. Rajakumar, C. Muralidharan, and V. Balasubramanian, Establishing Empirical Relationships to Predict Grain Size and Tensile Strength of Friction Stir Welded AA 6061-T6 Aluminium Alloy Joints, *Trans. Nonferr. Met. Soc.*, 2010, **20**, p 1863–1872
15. R.H. Myers and D.C. Montgomery, *Response Surface Methodology-Process and Product Optimization Using Designed Experiment*, Wiley, London, 1995
16. Design-Expert Software v8 User's Guide. Technical manual. Stat-Ease Inc, Minneapolis MN; 2010
17. ASTM E8 M-04 Standard test method for tension testing of metallic materials. ASTM International; 2006
18. ASTM G31-72 Standard practice for laboratory immersion corrosion testing of metals; 2002
19. T. Sivakumar, R. Manavalan, and C. Muralidharan, An Improvement HPLC Method with the Aid of a Chemometric Protocol: Simultaneous Analysis of Amlodipine and Atorvastatin in Pharmaceutical Formulations, *J. Sep. Sci.*, 2007, **30**, p 3143–3152
20. S. Rajakumar, C. Muralidharan, and V. Balasubramanian, Influence of Friction-Stir-Welding Process and Tool Parameters on Strength Properties of AA7075-T<sub>6</sub> Aluminium Alloy Joints, *Mater. Des.*, 2011, **32**, p 535–543

21. V. Balasubramanian, Relationship Between Base Metal Properties and Friction Stir Welding Process Parameters, *Mater. Sci. Eng. A*, 2009, **480**, p 397–403
22. K. Elangovan, V. Balasubramanian, and S. Babu, Developing an Empirical Relationship to Predict Tensile Strength of Friction Stir Welded AA2219 Aluminum Alloy, *J. Mater. Eng. Perform.*, 2008, **17**, p 820–830
23. X.H. Wang and K.S. Wang, Microstructure and Properties of Friction Stir Butt-Welded AZ31 Magnesium Alloy, *Mater. Sci. Eng. A*, 2006, **431**, p 114–117
24. K. Surekha, B.S. Murty, and K. Prasad Rao, Effect of Processing Parameters on the Corrosion Behaviour of Friction Stir Processed AA 2219 Aluminum Alloy, *Sol State Sci.*, 2009, **11**, p 907–917